ChemComm

COMMUNICATION

View Article Online
View Journal

Cite this: DOI: 10.1039/d2cc03219h

Received 7th June 2022,
Accepted 6th July 2022

DOI: 10.1039/d2cc03219h

rsc.li/chemcomm

Toggling the Z-type interaction off-on in nickel-boron dihydrogen and anionic hydride complexes†

Jacob R. Prat,[a] Ryan C. Cammarota,[a] Brendan J. Graziano,[a] James T. Moore[a] and Connie C. Lu *[ab]

Completing a series of nickel-group 13 complexes, a coordinatively unsaturated nickel-boron complex and its derivatives with a H_2, N_2, or hydride ligand were synthesized and characterized. The toggling "on" of a Ni(0)–B(III) inverse-dative bond enabled the stabilization of a nickel-bound anionic hydride with a remarkably low thermodynamic hydricity of $\Delta G^\circ_{H^-} = 21.4 \pm 1.0$ kcal mol^{-1} in THF. The flexible topology of the boron metalloligand confers both favorable hydrogen binding affinity and strong hydride donicity, albeit at the cost of high H_2 basicity during deprotonation to form the hydride.

Organic hydride donors are ubiquitous in organic transformations and are readily tuned to produce a wide range of hydride donor abilities.[1] However, the lack of regenerable, strongly hydridic reagents is a current hurdle that limits catalytic applicability. Transition metal hydrides, on the other hand, are regenerable from H_2 and are widely used in catalysis. However, only a few precious metal hydride complexes are able to match the lowest hydricity values exhibited by the strongest organic hydride donors, such as trialkylborohydrides ($\Delta G^\circ_{H^-}$ ~20 to 26 kcal mol^{-1} in CH_3CN).[1,2] Frustrated Lewis pairs, where main-group-based Lewis acid-base pairs facilitate H_2 heterolysis, also catalyze difficult hydrogenation reactions and represent another alternative strategy to avoid precious metals.[1b,3]

Within the last decade the use of a Lewis acidic borane as a supporting moiety[4] has proven to be an effective strategy in bolstering first-row transition metal-based H_2 and hydride reactivity.[5] We have found that bonding a heavy group 13 center (Al, Ga, In) to a d^{10} nickel atom engenders catalytic hydrogenation reactivity.[6,8b] Despite precedence in the literature,[7] the Ni–B pairing has until now remained elusive in our double-decker ligand scaffold, $[N((o\text{-}C_6H_4)NCH_2P^iPr_2)_3]^{3-}$ (abbrev. L^{3-}).[8] Herein we report the synthesis of a dinitrogen, dihydrogen, and hydride adduct of a nickel complex with the supporting boron metalloligand, BL. The anionic nickel hydride is the first example of a first-row metal complex with a thermodynamic hydricity lower than $HBEt_3^-$, while also deriving its hydride from H_2 heterolysis.

Initially, we pursued the synthesis of BL using similar protocols as those published for the heavier group 13 analogues,[8] which involved metalation of the ligand with various B(III) precursors. Unfortunately, these reactions showed incomplete substitution and/or formation of side products. An alternative strategy where the nickel atom is first installed in the trisphosphine pocket prior to the metallation of the supporting atom ultimately proved successful.[9] Heating $NiLi_3L$[9] with excess $B(OMe)_3$ yielded a red residue after workup (see ESI† for details). Gratifyingly, an X-ray diffraction study of a yellow crystal grown from pentane under N_2 at −25 °C revealed the complex to be the end-on N_2 adduct, (N_2)NiBL, or **1-N$_2$** (Scheme 1). A notable feature in the structure of **1-N$_2$** is the lack of any Ni–B interaction (Fig. 1A), as the Ni···B distance of 3.735(3) Å greatly exceeds the sum of the elements' atomic radii (2.36 Å).[10] The interaction of the B with the triarylamine base forms three fused five-membered rings. With the B positioned slightly below the triamido-plane, the three ligand arms are canted significantly outward. An unexpected consequence is the preclusion of a planar $Ni(P_3)$ unit, and instead, Ni is positioned 0.7280(5) Å above the P_3-plane. Such a geometric distortion is in stark contrast to that of $Ni(LH_3)$ and the heavier group 13 bimetallic congeners, NiAlL (**2**), NiGaL (**3**), and (N_2)NiInL (**4-N$_2$**), which all have a nearly planar $Ni(P_3)$ unit and shorter Ni–P_3-plane distances (0.03 to 0.38 Å).[8b,11] With N_2 in the apical pocket, the Ni center in **1-N$_2$** has an ideal tetrahedral geometry (τ'_4 = 0.98).[12] The N–N bond length of 1.116(6) Å and the corresponding stretching frequency of 2065 cm^{-1} are indicative of a weakly activated N_2 ligand.[13] Of note, the N_2 ligand is more activated in **1-N$_2$** than in the

[a] Department of Chemistry, University of Minnesota, 207 Pleasant Street SE, Minneapolis, Minnesota 55455-0431, USA
[b] Institute of Inorganic Chemistry, University of Bonn, Gerhard-Domagk-Str. 1, 53121 Bonn, Germany. E-mail: clu@uni-bonn.de

† Electronic supplementary information (ESI) available: Experimental details for the synthesis, spectroscopic characterization, crystallographic data, and DFT calculations. CCDC 2132870–2132872. For ESI and crystallographic data in CIF or other electronic format see DOI: https://doi.org/10.1039/d2cc03219h

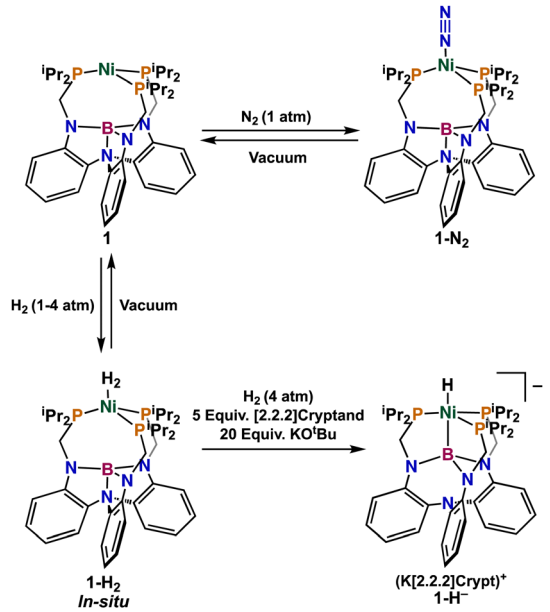

Scheme 1 Interconversions between **1**, **1-N$_2$**, and **1-H$_2$**, and the synthesis of **1-H$^-$**.

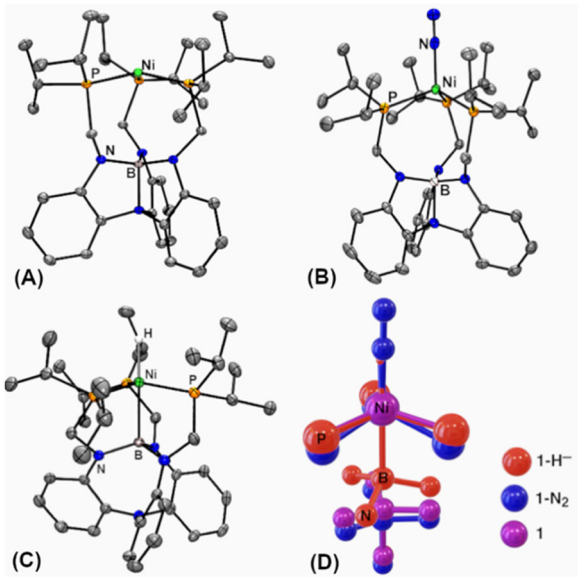

Fig. 1 Molecular structures of (A) **1**, (B) **1-N$_2$**, and (C) K(crypt-222)[**1-H**] plotted at 50% probability. Ligand hydrogen atoms and solvent molecules omitted for clarity. (D) Overlay of the first-coordination spheres for **1** (in purple), **1-N$_2$** (in blue), and **1-H$^-$** (in red).

analogous Ni–In complex (*c.f.* 2144 cm^{-1}), which is consistent with the Ni center being more electron-rich in the absence of a Z-type interaction.[6a,14]

Solutions of **1-N$_2$** exposed to vacuum or handled under argon allowed for the isolation of the coordinatively unsaturated NiBL, **1**. The ^{31}P{^{1}H} NMR shift of 23.9 ppm for **1-N$_2$** shifted upfield to 17.1 ppm after freeze–pump–thaw cycles, alongside a color change from yellow to bright red. An X-ray diffraction study of a crystal of **1** grown from a concentrated pentane solution at −35 °C revealed a long Ni–B distance of 3.380(4) Å, which is consistent with an absence of a direct bonding interaction. The Ni sits closer to the P$_3$-plane at 0.358 Å and has a pseudo trigonal pyramidal geometry (Σ(∡P–Ni–P) = 351.8°). No significant structural changes occurred at B, which is consistent with the observation of the same broad ^{11}B NMR peak at 17 ppm for both **1** and **1-N$_2$**.

Next, H$_2$ binding to **1** was investigated. Upon exposure to 1 atm H$_2$, a solution of **1** in C$_6$D$_6$ changed color from bright red to yellow and the ^{31}P{^{1}H} NMR peak shifted downfield to 31.7 ppm, while the ^{11}B NMR shift did not change appreciably. In the ^{1}H{^{31}P} NMR spectrum, a signal at 0.42 ppm that integrated to 2H and has a T$_1$(min) value of 13(2) ms at 400 MHz evidences an intact H$_2$ ligand and the formation of (η^2-H$_2$)NiBL, **1-H$_2$** (Fig. S23, ESI†).[15] Exposure of **1** to HD generated **1-HD** *in situ*, for which the J_{H-D} constant of 33 Hz provides an estimated H–D bond length of 0.89 Å (Fig. S24, ESI†).[16] The equilibrium for H$_2$ binding was then investigated using VT ^{31}P-NMR spectroscopy of **1** in THF-d_8 under 1 atm H$_2$ from 25 to 55 °C. The linear regression of the van't Hoff plot yielded the following thermodynamic values:[6a] ΔH° = −9.1(9) kcal mol^{-1}, ΔS° = −24(3) cal mol^{-1}·K, and ΔG° = −1.8(9) kcal mol^{-1}, where the standard state is defined as 1 atm H$_2$, 25 °C, and 1 M solutions for **1** and **1-H$_2$** (Fig. S25, ESI†).

To compare with the other Ni-group 13 bimetallics, the ΔG° for H$_2$ binding was also measured in toluene-d_8 (Fig. S27, ESI†). Ranking all the Ni-group 13 bimetallics in this ligand platform, the ΔG° for H$_2$ binding becomes increasingly exergonic in the following order (in kcal mol^{-1}): Ni–Al, 1.6(2) > Ni–Ga, 0.6(2) > Ni–B, −2.4(5) > Ni–In, −3.0(7).[17] Previously, our group and others had noted the strong correlation between ΔG° values and the Shannon ionic radius of the group 13 support.[6a,18] In contrast, the Ni–B variant bucks this trend, suggesting an electronic basis that is distinct from the others, for which increasing Ni–M Z-type interactions was proposed to facilitate H$_2$ binding. For the unique case of Ni–B, we propose that the significantly smaller B ion leads to ligand distortion that forces the Ni(P$_3$) unit to pyramidalize, which could also favor H$_2$ binding as a puckered Ni site would be more capable at π-backbonding and require less structural reorganization. The electron-richness of the Ni site in **1** is supported by its more negative oxidation potential ($E_{\frac{1}{2}}$ = −1.26 V *vs.* FeCp$_2^{+/0}$, Fig. S28 and Table S5, ESI†) relative to the other Ni-group 13 bimetallic complexes and even NiLH$_3$ (*c.f.* $E_{\frac{1}{2}}$ = −1.02 V *vs.* FeCp$_2^{+/0}$).[6a] A quasi-reversible reduction was also observed for **1** at −3.00 V *vs.* FeCp$_2^{+/0}$, which is similarly the most negative in the Ni-group 13 series.

Previously, adding a base to deprotonate the Ni-group 13 H$_2$ adducts enabled the isolation of rare d^{10} Ni hydride species.[19] Adding the strongly basic phosphazene, P$_4$^{t}Bu (pK_a^{CH3CN} = 42.7; pK_a^{THF} = 33.9)[20] to **1-H$_2$** in THF-d_8 under 1 atm of H$_2$, the anionic hydride complex, [HNiBL]$^-$ (**1-H$^-$**), was observed in equilibrium with **1-H$_2$**, alongside P$_4$^{t}Bu and its conjugate acid (Fig. S29, ESI†). By varying the base stoichiometry and monitoring the equilibrium for one week, the pK_a value for **1-H$_2$** was determined to be 36.0(2) in THF, with an estimated pK_a of

44.6(2) in CH_3CN. The characteristic ^1H NMR signal for the hydride was observed at −8.2 ppm as a broad complex multiplet. Upon applying ^{31}P decoupling the signal simplifies to a 1 : 1 : 1 : 1 quartet ($^2J_{H-B}$ = 26 Hz), showing coupling to the major ^{11}B nucleus. Applying ^{11}B decoupling gives roughly a 1 : 2 : 2 : 1 quartet ($^2J_{H-P}$ = 44 Hz), arising from coupling to the three P donors. Additionally, the sharp doublet ($^2J_{B-H}$ = 26 Hz) in the ^{11}B NMR spectrum at 22.7 ppm collapses to a singlet upon ^1H decoupling. Together, the data support a direct role of the B support in stabilizing the anionic Ni–H.

Single crystals of K(crypt-222)[**1-H**] were grown by combining **1**, excess KO^{t}Bu, and [2.2.2]cryptand in toluene under 4 atm H_2 and layering with pentane. The hydride ligand was located in the Fourier difference map with a Ni–H bond length of 1.56(2) Å (Fig. 1C). The solid-state structure of **1-H**$^-$ confirms a Z-type interaction between Ni and B with a Ni–B bond length of 2.235(2) Å, which is slightly on the long side when comparing to other Ni(0)-phosphine borane-appended complexes (range: 2.015–2.244 Å).[5a,7b,c] In a complimentary fashion, the B is positioned above the N_3 plane by 0.457(3) Å while the Ni–P_3 plane distance decreases to 0.3057(4) Å. To accommodate these changes, the ligand backbone contorts significantly, where the average P–Ni–B–N torsion angle of 34.5° is much greater than that for **1** and **1-N$_2$** (Fig. 1D and Table S2, ESI†).[11]

$$(H_2)M \rightleftharpoons H_2 + M \qquad \Delta G^\circ = -1.36\log(K_1) \qquad (1)$$

$$MH^- + HB^+ \rightleftharpoons (H_2)M + B \qquad \Delta G^\circ = -1.36\log(K_2) \qquad (2)$$

$$H^+ + B \rightleftharpoons HB^+ \qquad \Delta G^\circ = -1.36(pK_a) \qquad (3)$$

$$H_2 \rightleftharpoons H^+ + H^- \qquad \Delta G^\circ = 68.7_{(THF)}\ \text{kcal/mol} \qquad (4)$$

$$MH^- \rightleftharpoons M + H^- \qquad \Delta G^\circ_{H^-} \qquad (5)$$

The thermodynamic hydricity ($\Delta G^\circ_{H^-}$), or hydride donor ability, of **1-H**$^-$ can be determined from the thermochemical cycles shown in eqn (1)–(5) (Table S6, ESI†).[2b,21] Owing to the high basicity of **1-H$_2$**, the $\Delta G^\circ_{H^-}$ of **1-H**$^-$ is extremely low at 21.4 ± 1.0 kcal mol^{-1}, which can be converted to 16.7 ± 1.0 kcal mol^{-1} in CH_3CN (Table S9, ESI†). To the best of our knowledge, this hydricity value is the lowest reported for any transition metal hydride in organic solvents.[2b,21] The superior hydride donor ability exceeds that of many precious-metal hydrides and is on par with the estimated hydricity for the excited state of [IrCp*bpy(H)]$^+$.[2b,22] For experimental validation, we tested hydride-transfer reactions between **1** and strong hydride-donor reagents such as KHBEt$_3$, whose $\Delta G^\circ_{H^-}$ is 26 kcal mol^{-1} in CH_3CN.[2a] In line with the greater hydride donor ability of **1-H**$^-$, no reaction ensued. Even using a stronger hydride donor such as NaHB^{s}Bu$_3$, (predicted $\Delta G^\circ_{H^-}$ = 22.9 kcal mol^{-1}, Table S13, ESI†) did not result in any production of **1-H**$^-$. As further confirmation, isostructural [HNiAlL]$^-$ (**2-H**$^-$, $\Delta G^\circ_{H^-}$ = 26.2 kcal mol^{-1} in CH_3CN) was also incapable of transferring any hydride to **1**. On the other hand, the reverse reaction of **1-H**$^-$ and BEt$_3$ showed complete hydride transfer within minutes to provide **1** and HBEt$_3^-$ (Fig. S33-S37, ESI†). The closest reactivity in the literature was reported for the anionic H_2 adduct, [Na(THF)$_x$][P_3^BCo(H_2)], which transferred hydride to BEt$_3$ over the course of 20 h in 85% yield.[23] The combination of the $\Delta G^\circ_{H^-}$ of **1-H**$^-$, the reduction potential of **1**, and $E^\circ_{1/2}$ for the interconversion of a hydride ion and a hydrogen atom permits an estimation of the Ni–H bond dissociation free energy (BDFE) for **1-H**$^-$ of 66.7 ± 1.0 kcal mol^{-1} (Table S9, ESI†). Hence, **1-H**$^-$ is significantly more reactive for hydride transfer than H-atom transfer. Lastly, the Ni–H bond stretching frequency at ∼1565 cm^{-1} shifted to 1210 cm^{-1} upon deuteration (Fig. S42 and 43, ESI†).

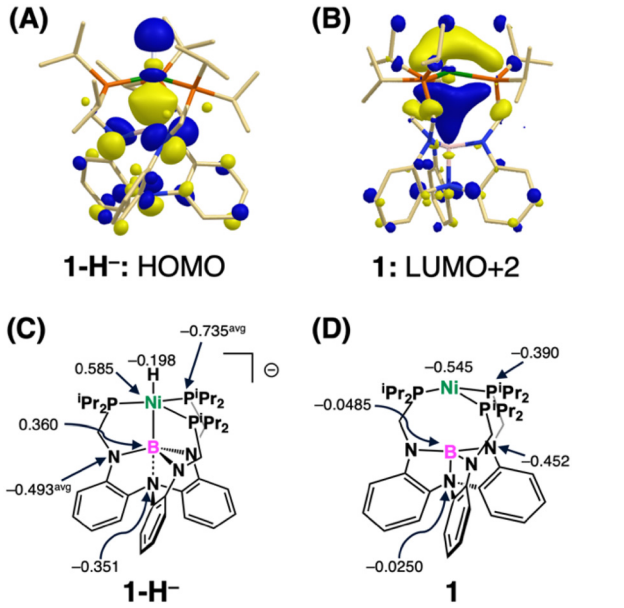

Fig. 2 DFT-calculated Kohn–Sham orbitals corresponding to: (A) the HOMO of **1-H**$^-$; and (B) the LUMO+2 of **1**. The Mulliken atomic charges of (C) **1-H**$^-$ and (D) **1**.

Turning to density functional theory (DFT), the Kohn–Sham orbital manifolds of **1-H**$^-$ and **1** were calculated (see ESI† for details).[19] The highest occupied molecular orbital (HOMO) of **1-H**$^-$ is a three-centered σ-bonding MO involving primarily the H(1s), Ni(3d$_{z^2}$), and B(2s/p) orbitals (Fig. 2A). Of note, Ni is bonding and antibonding with respect to B and H, respectively. A couple related MOs are a filled low-lying MO where the three atoms (Ni, B, and H) are σ-bonding and an unfilled MO that is fully σ*-bonding (Fig. S45, ESI†).

For **1**, a low-lying Ni-based acceptor orbital was found (LUMO+2, Fig. 2B). This MO has sizable contributions from Ni (4p$_z$, 13.5%) and the three P donors (3p$_z$, 20.7% total) when compared to the contribution from B (2s, 5.7%). Using the geometry of **1** as a starting point, we calculated a hypothetical anionic hydride congener to **1-H**$^-$ where the Z-type interaction is absent. The hypothetical hydride species was found to be 18.3 kcal mol^{-1} higher in enthalpy than **1-H**$^-$, highlighting the favorability of stabilizing the hydride *via* a *trans* Z-type ligand.

The addition of NiBL to the Ni–M series (M = B, Al, Ga, and In) allows us to better examine the effect of the identity of the Group 13 ion on H_2 binding, the pK_a of the H_2 ligand, and hydride donor ability (Table 1). The Ni–B system stands out in

Table 1 Thermodynamic values for the NiML series such as H_2 binding energies ($\Delta G^\circ_{H_2}$, kcal mol^{-1}), pK_a of H_2 adducts, and thermodynamic hydricity values ($\Delta G^\circ_{H^-}$, kcal mol^{-1})

NiML	1	2	3	4
M	B	Al	Ga	In
$\Delta G^\circ_{H_2}$ [a]	−2.4 (5)	1.6 (2)	0.6 (2)	−3.0 (7)
pK_a H_2 in THF	37.4 (2)	28.6 (1)	27.5 (3)	24.1 (1)
in CH_3CN	*44.6 (2)*	*36.7 (1)*	*33.1 (3)*	*31.9 (1)*
$\Delta G^\circ_{H^-}$ in THF	21.4 ± 1	31.8 ± 1	34.7 ± 1	39.2 ± 1
in CH_3CN	*16.7 ± 1*	*26.2 ± 1*	*31.3 ± 1*	*37.5 ± 1*

[a] In toluene.

the series for having the most basic H_2 adduct and the strongest hydride donor. Although the Ni–B system broke the observed correlation between the size of the Group 13 ion and ΔG° of H_2 binding (*vide supra*),[6a] a robust linear relationship was established between hydricity ($\Delta G^\circ_{H^-}$ in THF) and the Shannon ionic radii of the group 13 element (R^2 = 0.999, Table S12, ESI†). In other words, as the size of the group 13 ion increases, the Ni-hydride donor ability decreases. This trend is reasonable considering that the Ni–M Z-type interaction is intact in all the Ni hydrides in the series, which further underscores the importance of the group 13 identity as a σ-acceptor for stabilizing a *trans* anionic hydride. An inverse linear relationship was found between hydricity and the pK_a of the H_2 adduct (R^2 = 0.986, Fig. S46, ESI†). This suggests that the ease of deprotonating H_2 in our system depends more significantly on the stability of the hydride product, rather than the ΔG° of H_2 binding or the extent of H_2 activation.[24]

With the characterization of **1-H$_2$** and **1-H$^-$**, the hydride chemistry of trivalent group 13 bimetallic nickel complexes in this ligand scaffold has been extended. The Ni–B system further highlights the capability of "adaptable metalloboratranes",[4b,25] whereby the Z-type interaction can dynamically change to accommodate diverse reactive ligands at the transition metal. Studies of the application of the metal complexes with this unique binding paradigm are currently underway.

The authors thank the National Science Foundation (CHE-1954751) for support, Dr Matt Vollmer for experimental assistance, Dr Vic Young, Jr. (CHE-1229400) for X-ray crystallography assistance, and Dr Letitia Yao for NMR spectroscopy assistance. JRP was supported by the NSF Graduate Research Fellowship Program.

Conflicts of interest

There are no conflicts of interest to declare.

Notes and references

1 (*a*) S. Ilic, A. Alherz, C. B. Musgrave and K. D. Glusac, *Chem. Soc. Rev.*, 2018, **47**, 2809–2836; (*b*) D. W. Stephan, *J. Am. Chem. Soc.*, 2021, **143**, 20002–20014.
2 (*a*) M. T. Mock, R. G. Potter, D. M. Camaioni, J. Li, W. G. Dougherty, W. S. Kassel, B. Twamley and D. L. DuBois, *J. Am. Chem. Soc.*, 2009, **131**, 14454–14465; (*b*) K. R. Brereton, N. E. Smith, N. Hazari and A. J. M. Miller, *Chem. Soc. Rev.*, 2020, **49**, 7929–7948.
3 J. Lam, K. M. Szkop, E. Mosaferi and D. W. Stephan, *Chem. Soc. Rev.*, 2019, **48**, 3592–3612.
4 (*a*) H. Kameo, J. Yamamoto, A. Asada, H. Nakazawa, H. Matsuzaka and D. Bourissou, *Angew. Chem., Int. Ed.*, 2019, **58**, 18783–18787; (*b*) V. K. Landry, J. G. Melnick, D. Buccella, K. Pang, J. C. Ulichny and G. Parkin, *Inorg. Chem.*, 2006, **45**, 2588–2597; (*c*) B. R. Barnett, C. E. Moore, A. L. Rheingold and J. S. Figueroa, *J. Am. Chem. Soc.*, 2014, **136**, 10262–10265; (*d*) W. C. Shih, W. Gu, M. C. MacInnis, S. D. Timpa, N. Bhuvanesh, J. Zhou and O. V. Ozerov, *J. Am. Chem. Soc.*, 2016, **138**, 2086–2089; (*e*) A. J. Miller, J. A. Labinger and J. E. Bercaw, *J. Am. Chem. Soc.*, 2008, **130**, 11874–11875; (*f*) Y. Segawa, M. Yamashita and K. Nozaki, *J. Am. Chem. Soc.*, 2009, **131**, 9201–9203; (*g*) L. Yang, N. Uemura and Y. Nakao, *J. Am. Chem. Soc.*, 2019, **141**, 7972–7979.
5 (*a*) W. H. Harman and J. C. Peters, *J. Am. Chem. Soc.*, 2012, **134**, 5080–5082; (*b*) K. N. Tseng, J. W. Kampf and N. K. Szymczak, *J. Am. Chem. Soc.*, 2016, **138**, 10378–10381; (*c*) J. A. Zurakowski, B. J. H. Austen and M. W. Drover, *Organometallics*, 2021, **40**, 2450–2457.
6 (*a*) R. C. Cammarota, J. Xie, S. A. Burgess, M. V. Vollmer, K. D. Vogiatzis, J. Ye, J. C. Linehan, A. M. Appel, C. Hoffmann, X. Wang, V. G. Young, Jr. and C. C. Lu, *Chem. Sci.*, 2019, **10**, 7029–7042; (*b*) B. L. Ramirez and C. C. Lu, *J. Am. Chem. Soc.*, 2020, **142**, 5396–5407.
7 (*a*) M. Sircoglou, S. Bontemps, G. Bouhadir, N. Saffon, K. Miqueu, W. Gu, M. Mercy, C. H. Chen, B. M. Foxman, L. Maron, O. V. Ozerov and D. Bourissou, *J. Am. Chem. Soc.*, 2008, **130**, 16729–16738; (*b*) B. E. Cowie and D. J. H. Emslie, *Organometallics*, 2015, **34**, 4093–4101; (*c*) W. H. Harman, T. P. Lin and J. C. Peters, *Angew. Chem., Int. Ed.*, 2014, **53**, 1081–1086.
8 (*a*) P. A. Rudd, S. Liu, L. Gagliardi, V. G. Young, Jr. and C. C. Lu, *J. Am. Chem. Soc.*, 2011, **133**, 20724–20727; (*b*) R. C. Cammarota and C. C. Lu, *J. Am. Chem. Soc.*, 2015, **137**, 12486–12489.
9 J. R. Prat, C. A. Gaggioli, R. C. Cammarota, E. Bill, L. Gagliardi and C. C. Lu, *Inorg. Chem.*, 2020, **59**, 14251–14262.
10 (*a*) E. Clementi and D. L. Raimondi, *J. Chem. Phys.*, 1963, **38**, 2686; (*b*) Elements, Atomic Radii and the Periodic Radii, **http://crystalmaker.com/support/tutorials/atomic-radii/index.html**.
11 R. J. Eisenhart, L. J. Clouston and C. C. Lu, *Acc. Chem. Res.*, 2015, **48**, 2885–2894.
12 D. Rosiak, A. Okuniewski and J. Chojnacki, *Polyhedron*, 2018, **146**, 35–41.
13 P. L. Holland, *Dalton Trans.*, 2010, **39**, 5415–5425.
14 M. V. Vollmer, J. Xie and C. C. Lu, *J. Am. Chem. Soc.*, 2017, **139**, 6570–6573.
15 (*a*) M. T. Bautista, K. A. Earl, P. A. Maltby, R. H. Morris, C. T. Schweitzer and A. Sella, *J. Am. Chem. Soc.*, 2002, **110**, 7031–7036; (*b*) R. H. Crabtree, *Angew. Chem., Int. Ed. Engl.*, 1993, **32**, 789–805; (*c*) R. H. Morris and R. J. Wittebort, *Magn. Reson. Chem.*, 1997, **35**, 243–250.
16 (*a*) P. A. Maltby, M. Schlaf, M. Steinbeck, A. J. Lough, R. H. Morris, W. T. Klooster, T. F. Koetzle and R. C. Srivastava, *J. Am. Chem. Soc.*, 1996, **118**, 5396–5407; (*b*) T. A. Luther and D. M. Heinekey, *Inorg. Chem.*, 1998, **37**, 127–132; (*c*) G. J. Kubas, *Chem. Rev.*, 2007, **107**, 4152–4205.
17 (*a*) R. C. Cammarota, University of Minnesota, 2018; (*b*) M. V. Vollmer, University of Minnesota, 2019. See **https://conservancy.umn.edu/**.
18 D. You and F. P. Gabbaï, *Trends Chem.*, 2019, **1**, 485–496.
19 R. C. Cammarota, M. V. Vollmer, J. Xie, J. Ye, J. C. Linehan, S. A. Burgess, A. M. Appel, L. Gagliardi and C. C. Lu, *J. Am. Chem. Soc.*, 2017, **139**, 14244–14250.
20 S. Tshepelevitsh, A. Kutt, M. Lokov, I. Kaljurand, J. Saame, A. Heering, P. G. Plieger, R. Vianello and I. Leito, *Eur. J. Org. Chem.*, 2019, 6735–6748.
21 E. S. Wiedner, M. B. Chambers, C. L. Pitman, R. M. Bullock, A. J. Miller and A. M. Appel, *Chem. Rev.*, 2016, **116**, 8655–8692.
22 S. M. Barrett, C. L. Pitman, A. G. Walden and A. J. Miller, *J. Am. Chem. Soc.*, 2014, **136**, 14718–14721.
23 M. M. Deegan, K. I. Hannoun and J. C. Peters, *Angew. Chem., Int. Ed.*, 2020, **59**, 22631–22637.
24 R. H. Morris, *J. Am. Chem. Soc.*, 2014, **136**, 1948–1959.
25 M. E. Moret and J. C. Peters, *Angew. Chem., Int. Ed.*, 2011, **50**, 2063–2067.

